HHS Public Access

Author manuscript

Biochem Biophys Res Commun. Author manuscript; available in PMC 2017 February 12.

Published in final edited form as:

Biochem Biophys Res Commun. 2016 February 12; 470(3): 613–619. doi:10.1016/j.bbrc.2016.01.096.

Postnatal lethality and abnormal development of foregut and spleen in *Ndrg4* mutant mice

Xianghu Qu[1,#], **Jing Li**[1], and **H. Scott Baldwin**[1,2]

[1]Department of Pediatrics (Cardiology), Vanderbilt University Medical Center, Nashville, TN 37232, USA

[2]Department of Cell and Development Biology, Vanderbilt University Medical Center, Nashville, TN 37232, USA

Abstract

NDRG4 is a member of the *NDRG* family (N-myc downstream-regulated gene), which is highly expressed in brain and heart. Previous studies showed that *Ndrg1*-deficient mice exhibited a progressive demyelinating disorder of peripheral nerves and *Ndrg4*-deficient mice had spatial learning deficits and vulnerabilities to cerebral ischemia. Here, we report generation of *Ndrg4* mutant alleles that exhibit several development defects different from those previously reported. Our homozygous mice showed growth retardation and postnatal lethality. Spleen and thymuses of $Ndrg4^{-/-}$ mice are considerably reduced in size from 3 weeks of age. Histological analysis revealed abnormal hyperkeratosis in the squamous foregut and abnormal loss of erythrocytes in the spleen of $Ndrg4^{-/-}$ mice. In addition, we observed an abnormal hind limb clasping phenotype upon tail suspension suggesting neurological abnormalities. Consistent to these abnormalities, Ndrg4 is expressed in smooth muscle cells of the stomach, macrophages of the spleen and neurons. Availability of the conditional allele for *Ndrg4* should facilitate further detailed analyses of the potential roles of Ndrg4 in gut development, nervous system and immune system.

Keywords

Growth retardation; Hyperkeratosis; Erythrocyte; Conditional knockout

1. Introduction

Cytoplasmic protein Ndrg4 belongs to the N-myc downstream regulated gene (NDRG) family, which consists of four related members, NDRG1-NDRG4, in mammals and are well conserved through evolution [1–2]. The proteins consist of 325–394 amino acid residues, and share 53–65% sequence identity with each other [3]. Although the precise molecular and cellular function of these NDRG members has not been fully elucidated, emerging

[#]Correspondence: Xianghu Qu, Ph.D., Division of Pediatric Cardiology, Vanderbilt University Medical Center, 9435-A MRB IV-Langford, 2213 Garland Ave., Nashville, TN 37232-0493, Ph: 615.322.2703, Fax: 615.322.6541, Xianghu.qu@vanderbilt.edu.

evidence implicates their roles in development, cancer metastasis, and the immune system [4–8]. The first described mouse mutant model for this family was *NDRG1*-deficient mice, which were unable to maintain myelin sheaths in peripheral nerves [9]. This phenotype was consistent with human hereditary motor and sensory neuropathy, Charcot-Marie-Tooth disease type 4D, caused by a nonsense mutation of *NDRG1* [10]. *NDRG2*-deficient (*NDRG2*$^{-/-}$) mice were recently reported to be viable and fertile without apparent physical abnormalities, but had a markedly shorter lifespan than the wild-type (wt) or *NDRG2*$^{+/-}$ mice, and they are susceptible to tumor formation, including lymphoma, hepatocellular carcinoma and bronchoalveolar carcinoma, suggesting that NDRG2 is a possible tumour suppressor in various types of cancer [11]. In addition, loss of *Ndrg2* in mice resulted in vertebral homeotic transformations in thoracic/lumbar and lumbar/sacral transitional regions in a dose-dependent manner [12].

An *NDRG4*-deficient mouse model was previously described [13]. Although the homozygous mutant mice were born at normal Mendelian ratios, they showed impaired phenotypes in spatial learning and memory, and neuroprotection with decreased levels of brain-derived neurotrophic factor. Here, we have generated mice with a conditional allele for the *Ndrg4* gene. When a global null mutation for the *Ndrg4* gene was generated from the floxed mice, to our surprise, we observed several more severe phenotypes different from those previously reported: an abnormal hind limb clasping phenotype and growth retardation with disproportional small spleens and thymuses from the age of about 3 weeks. In addition, our homozygous mutant *Ndrg4*$^{-/-}$ mice also exhibited partial postnatal lethality. In agreement with reduced size in the forestomach and the spleen of *Ndrg4* mutant mice, we observed abnormal hyperkeratosis in the squamous foregut and abnormal loss of erythrocytes in the spleen of *Ndrg4*$^{-/-}$ mice. We also detected a considerable Ndrg4 expression in stomach, spleen and neurons of wt mice.

2. Methods

2.1. Mouse Breeding and Generation of *Ndrg4* Mutant Alleles

All strains were maintained on a mixed 129 and C57/BL6 background. The animals were handled in accordance with institutional guidelines with the approval of the Institutional Animal Care and Use Committee of Vanderbilt University School of Medicine. The authors are currently exploring possibilities to deposit the newly developed mice to public repositories and are happy to share them upon request.

To identify tissue-specific functions of Ndrg4, we have created a conditional allele of the mouse *Ndrg4* gene by introducing Cre recombinase recognition sites (*loxP*) into the *Ndrg4* locus. This strategy involved introducing a *loxP* site and a neomycin resistance cassette within the intron 5, and another *loxP* site into the intron 7 (Fig. 1a), such that Cre recombination excises the *Ndrg4* exon 5-7 leading reading frame shift. A *Ndrg4* floxed targeting vector was constructed based on the 129-Sv mouse genomic fragment. A 744bp *Hpa*I-*Ase*I fragment containing *Ndrg4* exons 6-8 was inserted into the Floxed *Kpn*I-*Cla*I sites of the pDELBOY plasmid [14], which contains an *Frt*-site-flanked neomycin gene expressed from the phosphoglycerate kinase promoter (*PGK-neo*), two *loxP* sites and a cassette containing the herpes simplex virus thymidine kinase gene expressed from the

phosphoglycerate kinase promoter (*PGK-HSV-tk*). Also, a 2.9-kb *Ase*I-*Bam*HI fragment (3′ short arm) and a 3.7-kb *Sal*I-*Hpa*I fragment (5′ long arm) were respectively inserted into the *Xho*I site and the *Sal*I site of this construct. The targeting vector was linearized with *Not*I and electroporated into G4 hybrid mouse embryonic stem (ES) cell line, which was established from male blastocyst derived from the natural mating of 129S6/SvEvTac female with C57BL/6Ncr male in the Nagy lab [15]. The correct gene targeting was confirmed by Southern blot with both 5′ and 3′ external probes (Fig. 1b). Presence of the 5′ loxP site was confirmed by genomic PCR using primers P1 (5′-TAGGCAGGGGCAGGTGGGTTTGT-3′) and P2 (5′-GGCGTCTCGATGTCATGTTCCTGT-3′). Targeted cells were then injected into C57/BL6 blastocysts and two of the resulting chimeras were found to transmit the targeted allele through the germline. Both lines were maintained on a 129 and C57/BL6 background and showed the same phenotype. Then, the neo cassette was removed by crossing with *ROSA26-Flp* transgenic mice to generate heterozygous mice for the floxed allele without neo (+/*fx*) (Farley *et al*., 2000). The resulting heterozygous floxed *Ndrg4* mutant mice ($Ndrg4^{+/fx}$) were interbred to make homozygous for the conditional allele (*fx*/*fx*). To make global *Ndrg4* knockout mice, the $Ndrg4^{+/fx}$ mice were crossed with *E2A-cre* transgenic mice, which express the Cre recombinase in germ cells [16]. Cre-dependent deletion was detected with primers P1, P2 and P3 (5′-GCTCCCACTCCAATGCCAATC-3′) (Fig. 1a, c). The resulting $Ndrg4^{+/-}$ mice were intercrossed to generate homozygous *Ndrg4* mutant mice.

2.2. Histological and Western Blot Analysis

Stomach and spleen were fixed in 4% paraformaldehyde (PFA), embedded in paraffin and stained with hematoxylin and eosin (H&E) according to a standard procedure. For Western blotting, brains and hearts were homogenized in a dounce homogenizer using modified radio-immunoprecipitation assay (RIPA) buffer (50 mM Tris-HCl [pH 7.5], 150 mM NaCl, 1 mM EDTA [pH 8.0], 1% NP-40, 0.5% Na deoxycholate, 0.1% sodium dodecyl sulfate [SDS]) supplemented with Complete Protease Inhibitors (Roche Diagnostics) and centrifuged at 12,000g for 12 min. Lysates were subjected to Western blot analysis using standard technologies. The western blots were probed with the primary antibody (mouse monoclonal anti-NDRG4, clone 2G3, Novus Biologicals, T5168), followed by treatment with HRP-conjugated goat anti-mouse IgG (Promega, W4021). Positive signals were visualized using a Pierce ECL western blotting substrate detection Kit (Pierce, 32132). For normalization of signals, mouse anti-α-Tublin (clone B-5-1-2, Sigma, H00065009-M01) monoclonal antibody was used as a loading control.

2.3. Immunohistochemistry and Antibodies

Immunostaining was performed on frozen sections as previously described [14]. Briefly, spleen and stomach were dissected, fixed in 4% PFA in phosphate-buffered saline (PBS, pH 7.4) overnight at 4°C, washed with PBS, and cryoprotected with 30% sucrose in PBS overnight; embedded in OCT and then cryosectioned at 10μm. The frozen sections were stained with the following primary antibodies and conjugates: rat monoclonal (RA3-6B2) anti-B220 (eBioscience, 14-0452), Fluorescein isothiocyanate (FITC) rat monoclonal (4E3) anti-CD21/CD35 (eBioscience, 11-0212), Alex Fluor 647 anti-mouse CD4 (eBioscience, 51-0041), rat monoclonal (ER-TR9) anti-SIGN Related 1 (SIGN R1) (eBioscience,

ab37220), FITC anti-Mucosal vascular addressin-1 (MAdCAM1) (eBioscience, 11-5997), and Allophycocyanin (APC) anti-mouse TER-119 (eBioscience, 17-5921), rat monoclonal anti-ER-TR-7 (Santa Cruz, sc-73355), rat monoclonal (CL:A3-1) anti-F4/80 (abcam, ab6640), rabbit anti-NDRG4 antibody (N13) [16] and Cy3 conjugated anti-α-Smooth Muscle Actin (SMA) (Sigma, C-6198). Hippocampus neurons were isolated from E17.5 wt embryos, cultured for 35 days and then stained with antibodies for Ndrg4 and α-Tublin. For the non-conjugated primary antibodies, Alexa Fluor 488 and 594 fluorochrome-conjugated secondary antibodies (Invitrogen) were used for signal detection. Images were acquired on an Olympus fluorescent microscope or with a Leica TCS SP2 confocal system (Leica Microsystems), and processed in Adobe Photoshop.

2.4. Measurements of Fasted Blood Glucose Concentrations in Mice

After overnight fasting, blood was obtained from tails (5 mice/genotype), and glucose concentrations were measured using a glucometer (One Touch Ultra; Johnson & Johnson).

2.5. Statistical Analysis

Data are expressed as the means ± the standard error of the mean. Statistical analysis was conducted using the 2-tailed Student's t-test. A P value < 0.05 was considered significant.

3. Results and discussion

We and other labs originally documented that *Ndrg4* is abundantly expressed in the murine brain and heart [1,3,18] and that *Ndrg4* is essential for normal cardiac development in zebra fish [4]. To elucidate the effects of *Ndrg4* deficiency *in vivo* and allow temporal and tissue-specific gene inactivation, we have created a conditional allele of the mouse *Ndrg4* gene. We flanked the *Ndrg4* exon 5-7 with two *loxP* sites (Fig. 1a), such that Cre recombination excises the *Ndrg4* exon 5-7 leading reading frame shift. We verified homologous recombination at the gene-targeted locus in G4 ES cells [15] and mutant mice by Southern blot hybridization (Fig. 1b) and genomic PCR (Fig. 1c). Then, mice heterozygous for the $Ndrg4^{fx\text{-}neo}$ allele were mated with *FLPe* transgenic mice ubiquitously expressing *Flp*-recombinase [19] to remove the *PGK-neo* gene, thus generating heterozygous $Ndrg4^{+/fx}$ mice. The latter were intercrossed to generate homozygous $Ndrg4^{fx/fx}$ mice. This cross resulted in normal litter sizes and Mendelian distributions of genotypes. Homozygous floxed *Ndrg4* mice ($Ndrg4^{fx/fx}$) developed normally and show no obvious abnormalities and are fertile. Their levels of *Ndrg4* expression were indistinguishable from those of wt animals. To make global *Ndrg4* knockout mice, the $Ndrg4^{+/fx}$ mice were crossed with *E2A-cre* transgenic mice, which express the Cre recombinase in germ cells [16]. The resulting $Ndrg4^{+/-}$ mice are overtly as normal as wt. When the $Ndrg4^{+/-}$ mice were intercrossed, all three possible genotypes were born with normal Mendelian frequency. We confirmed the elimination of Ndrg4 expression in the brain and heart, where Ndrg4 is abundantly expressed in wt mice (Fig. 1d). Thus, the *Ndrg4* gene was effectively disrupted.

Although indistinguishable at birth, to our surprise, beginning around 3 weeks of age all of the homozygous $Ndrg4^{-/-}$ mice exhibited an abnormal hind limb clasping phenotype upon tail suspension, suggesting neurological abnormalities (Fig. 2b, c), reminiscent of the

phenotype in the adult *Ndrg1*-deficient mice [9], but not observed in the previously described *Ndrg4*-deficient model [13]. At the same time, we observed severe growth retardation of the *Ndrg4*$^{-/-}$ mice. Compared to wt control littermates, the body weight of *Ndrg4*$^{-/-}$ mice was reduced by 6%–12% within 2 weeks after birth. Thereafter, the body weight reduction became more severe with *Ndrg4*$^{-/-}$ mice weighing 30% less at weaning, 42.8% less at 4 weeks when compared to wild type mice (Fig. 2a, d). In addition, 20.7% (12 of 58) of *Ndrg4*$^{-/-}$ mice (n=58) died between 3 and 6 weeks after birth. 69.2% (9 of 13) died between 12–16 months after birth (Fig. 2e). Those animals that survived past 16 months could gain weight to adulthood, but after several months they were still smaller than their wt siblings.

Necropsy revealed that the size of each organ of *Ndrg4*$^{-/-}$ mice including heart and brain (Fig. 2f–h) was proportional to the body dimensions, except foregut, spleen and thymuses. From about 3 weeks of age, all the *Ndrg4*$^{-/-}$ mice had disproportional small spleens and marked foregut shrinkage, about ¾ of *Ndrg4*$^{-/-}$ mice also had disproportional small thymuses and mucosa-associated lymphoid tissues, such as Peyer's patches (PP) (Fig. 2i–p). Histological analysis revealed hyperkeratosis in the squamous foregut (Fig. 3a–f), but no cellular or morphological abnormalities in the intestine and glandular stomach in the mutant mice (data not shown). Hyperkeratosis in the squamous foregut was first detected at about 2 weeks of age (Fig. 3a–d) and becomes more severe at weaning (Fig. 3e, f). Histological examination of other keratinized tissues (esophagus and skin) detected no obvious hyperkeratosis (data not shown). Given the perturbations of the foregut anatomy in *Ndrg4*$^{-/-}$ mice, we wanted to determine if there was an associated digestion disorder. Comparison of blood glucose levels between wt littermates (n=5), adult *Ndrg4*$^{-/-}$ mice (n=5) demonstrated a reduced blood sugar level (6.36±0.82 vs 4.04±0.90 mmol/L) (Fig. 3g) in *Ndrg4*$^{-/-}$ mice suggestive of malnutrition.

We have also examined histological sections of splenic tissue. The spleens from wt and *Ndrg4*$^{-/-}$ mice both show defined white pulp regions, which are concentrated areas of lymphocytes and is dark blue after H&E staining. However, the red pulp, which contains mainly erythrocytes, had a much lower cell density in *Ndrg4* mutants than seen in wt controls (Fig. 4a–d). Further immunohistochemistry with antibodies against specific cell markers confirmed dramatic loss of healthy erythrocytes and abnormal accumulation of damaged red blood cells (Fig. 4s, t). Although, as in wild-type spleens, the white pulp (wp) is sharply separated from the red pulp (rp) with clear marginal zone (Fig. 4m–p) and normal morphology of the reticular meshwork in RP (data no shown) in both wt and mutant animals. Similarly B cells, T cells, follicular dendritic cells and macrophages were all normally localized in the mutant spleens (Fig. 4e–l, q, r).

Given neurological abnormalities and the defects in the stomach and spleen of the *Ndrg4* mutant mice, we wanted to know whether Ndrg4 is expressed in these organs. Cryostat sections of stomach (a–c) of wild-type mice were co-immunostained with Ndrg4 antibody and SMA (smooth muscle cell marker) and revealed that Ndrg4 is highly expressed in smooth muscle cells of forestomach (Supplemental Fig. 5a–c) and glandular stomach, with weaker expression in epithelial cells (data not shown). In spleen, Ndrg4 is co-localized with pan-macrophage marker F4/80, indicating its expression in macrophage cells of the spleen.

In addition, Ndrg4 is also expressed in hippocampus neurons at E17.5 (Supplemental Fig. 1g, h).

Taken together, our current *Ndrg4* mutant mice exhibit more severe phenotypes than those previously reported [13]: neurological abnormalities, growth retardation, postnatal lethality (shorter lifespan), disproportional small spleens and thymuses, abnormal hyperkeratosis in the foregut and abnormal loss of erythrocytes in the spleen. The significant differences in phenotypes between the two mutant models are probably related to: 1) variations of the genetic background, 2) different gene-targeting strategies, 3) multiple isoforms of Ndrg4 (all the known isoforms were disrupted in our null model). We believe that growth retardation and early death of mutant animals is most likely caused by the observed gut defects. We suspect that malnutrition results from hyperkeratosis in the foregut. But we cannot exclude the presence of other crucial defects in $Ndrg4^{-/-}$ mice. Indeed, Ndrg1-4 are co-expressed in many tissues [3,18], and they may have both distinct and overlapping function.

Since spleen function is not essential for survival it has two main functions. The first is to provide a proper microenvironment to lymphoid and myeloid cells and the second involves clearance of abnormal erythrocytes. The latter function was clearly disrupted in the $Ndrg4^{-/-}$ mice. In addition, the spleen transiently exhibits erythropoietic activity similar to the liver during fetal life. Given that targeted disruption of the *Ndrg4* gene in mice results in abnormalities in the spleen and thymus, as well as neurological defects, our conditional allele for *Ndrg4* should facilitate further detailed analyses of the potential roles of Ndrg4 in nervous system and immune system.

Supplementary Material

Refer to Web version on PubMed Central for supplementary material.

Acknowledgments

We thank Dr. Koichi Kokame (National Cerebral and Cardiovascular Center, Osaka, Japan) for generously sharing their rabbit anti-NDRG4 antibody (N13) with us. This work was supported by National Institutes of Health grants R01 HL86964 (H.S.B.)

Abbreviations

NDRG	N-myc downstream regulated gene
ES	embryonic stem
PP	Peyer’s patches
wt	wild-type
wp	white pulp
rp	red pulp

References

1. Zhou RH, Kokame K, Tsukamoto Y, Yutani C, Kato H, Miyata T. Characterization of the human NDRG gene family: a newly identified member, NDRG4, is specifically expressed in brain and heart. Genomics. 2001; 73:86–97. [PubMed: 11352569]
2. Melotte V, Qu X, Ongenaert M, van Criekinge W, de Bruïne AP, Baldwin HS, van Engeland M. The N-myc downstream regulated gene (NDRG) family: diverse functions, multiple applications. FASEB J. 2010; 24:4153–4166. [PubMed: 20667976]
3. Qu X, Zhai Y, Wei H, Zhang C, Xing G, Yu Y, He F. Characterization and expression of three novel differentiation-related genes belong to the human NDRG gene family. Mol Cell Biochem. 2002; 229:35–44. [PubMed: 11936845]
4. Qu X, Jia H, Garrity DM, Tompkins K, Batts L, Appel B, Zhong TP, Baldwin HS. Ndrg4 is required for normal myocyte proliferation during early cardiac development in zebrafish. Dev Biol. 2008; 317:486–496. [PubMed: 18407257]
5. Taketomi Y, Sunaga K, Tanaka S, Nakamura M, Arata S, Okuda T, Moon TC, Chang HW, Sugimoto Y, Kokame K, Miyata T, Murakami M, Kudo I. Impaired mast cell maturation and degranulation and attenuated allergic responses in Ndrg1-deficient mice. J Immunol. 2007; 178:7042–7053. [PubMed: 17513753]
6. King RH, Chandler D, Lopaticki S, Huang D, Blake J, Muddle JR, Kilpatrick T, Nourallah M, Miyata T, Okuda T, Carter KW, Hunter M, Angelicheva D, Morahan G, Kalaydjieva L. Ndrg1 in development and maintenance of the myelin sheath. Neurobiol Dis. 2011; 42:368–380. [PubMed: 21303696]
7. Benesh EC, Miller PM, Pfaltzgraff ER, Grega-Larson NE, Hager HA, Sung BH, Qu X, Baldwin HS, Weaver AM, Bader DM. Bves and NDRG4 regulate directional epicardial cell migration through autocrine extracellular matrix deposition. Mol Biol Cell. 2013; 24:3496–3510. [PubMed: 24048452]
8. Ichikawa T, Nakahata S, Fujii M, Iha H, Morishita K. Loss of NDRG2 enhanced activation of the NF-κB pathway by PTEN and NIK phosphorylation for ATL and other cancer development. Sci Rep. 2015; 5:12841. [PubMed: 26269411]
9. Okuda T, Higashi Y, Kokame K, Tanaka C, Kondoh H, Miyata T. Ndrg1-deficient mice exhibit a progressive demyelinating disorder of peripheral nerves. Mol Cell Biol. 2004; 24:3949–3956. [PubMed: 15082788]
10. Kalaydjieva L, Gresham D, Gooding R, Heather L, Baas F, de Jonge R, Blechschmidt K, Angelicheva D, Chandler D, Worsley P, Rosenthal A, King RH, Thomas PK. N-myc downstream-regulated gene 1 is mutated in hereditary motor and sensory neuropathy-Lom. Am J Hum Genet. 2000; 67:47–58. [PubMed: 10831399]
11. Nakahata S, Ichikawa T, Maneesaay P, Saito Y, Nagai K, Tamura T, Manachai N, Yamakawa N, Hamasaki M, Kitabayashi I, Arai Y, Kanai Y, Taki T, Abe T, Kiyonari H, Shimoda K, Ohshima K, Horii A, Shima H, Taniwaki M, Yamaguchi R, Morishita K. Loss of NDRG2 expression activates PI3K-AKT signalling via PTEN phosphorylation in ATLL and other cancers. Nat Commun. 2014; 26:3393. [PubMed: 24569712]
12. Zhu H, Zhao J, Zhou W, Li H, Zhou R, Zhang L, Zhao H, Cao J, Zhu X, Hu H, Ma G, He L, Yao Z, Yao L, Guo X. Ndrg2 regulates vertebral specification in differentiating somites. Dev Biol. 2012; 369:308–318. [PubMed: 22819676]
13. Yamamoto H, Kokame K, Okuda T, Nakajo Y, Yanamoto H, Miyata T. NDRG4 Protein-deficient Mice Exhibit Spatial Learning Deficits and Vulnerabilities to Cerebral Ischemia. J Biol Chem. 2011; 286:26158–26165. [PubMed: 21636852]
14. Qu X, Tompkins K, Batts LE, Puri M, Baldwin HS. Abnormal embryonic lymphatic vessel development in Tie1 hypomorphic mice. Development. 2010; 137:1285–1295. [PubMed: 20223757]
15. George SH, Gertsenstein M, Vintersten K, Korets-Smith E, Murphy J, Stevens ME, Haigh JJ, Nagy A. Developmental and adult phenotyping directly from mutant embryonic stem cells. Proc Natl Acad Sci USA. 2007; 104:4455–4460. [PubMed: 17360545]

16. Lakso M, Pichel JG, Gorman JR, Sauer B, Okamoto Y, Lee E, Alt FW, Westphal H. Efficient in vivo manipulation of mouse genomic sequences at the zygote stage. Proc Natl Acad Sci USA. 1996; 93:5860–5865. [PubMed: 8650183]
17. Nishimoto S, Tawara J, Toyoda H, Kitamura K, Komurasaki T. A novel homocysteine-responsive gene, smap8, modulates mitogenesis in rat vascular smooth muscle cells. Eur J Biochem. 2003; 270:2521–2531. [PubMed: 12755708]
18. Okuda T, Kokame K, Miyata T. Differential expression patterns of NDRG family proteins in the central nervous system. J Histochem Cytochem. 2008; 56:175–182. [PubMed: 17998568]
19. Farley FW, Soriano P, Steffen LS, Dymecki SM. Widespread recombinase expression using FLPeR (flipper) mice. Genesis. 2000; 28:106–110. [PubMed: 11105051]

Highlights

This Ndrg4 mutant allele is the first conditional allele in this family of genes.

Ndrg4$^{-/-}$ mice showed growth retardation and shorter lifespan.

Neurological abnormalities, disproportional small spleens and thymuses in *Ndrg4*$^{-/-}$ mice.

Abnormal hyperkeratosis in the foregut and abnormal loss of erythrocytes in the spleen of *Ndrg4*$^{-/-}$ mice.

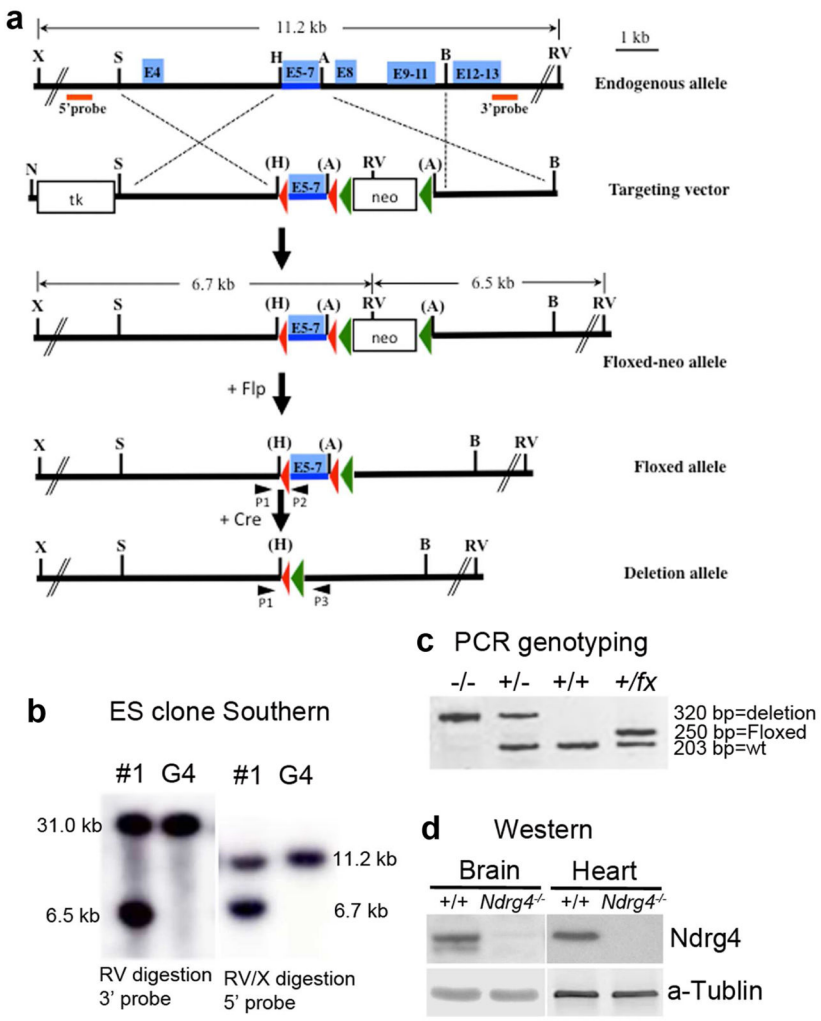

Fig. 1.

Generation of *Ndrg4* mutant lines. **(a)** Schematic representation of the targeting strategy and deleting *Ndrg4* exons 5-7 in mice. Top: *Ndrg4* genomic structure. The targeting vector was designed so that *loxP* sites would flank the 744bp *Hpa*I-*Ase*I fragment containing *Ndrg4* exons 5-7. Homologous recombination with the targeting vector generated the *flox-neo* allele; Flp deletion created the floxed allele; subsequent Cre deletion led to the deletion allele. Blue boxes, exons; red boxes, external probes for Southern blot analysis (diagnostic band lengths pre/post-recombination indicated); neo, Neomycin resistance cassette; TK, thymidine kinase cassette. Red and green arrowheads indicate *LoxP* and *Frt* sites, respectively. A, *Ase*I; B, *Bam*HI; H, *Hpa*I; N, *Not*I; RV, *Eco*RV; S, *Sal*I; X, *Xho*I. Primers used for isolation of correctly targeted ES cells and for routine genotyping are indicated by small arrows. **(b)** Southern blot analysis of the parental (G4) and correctly targeted ES cell clones using the probes depicted in **(a)**. *Eco*RV-digested DNA was hybridized to a 3′ flanking probe (3′probe): A 31.0-kb band was observed for the wild-type allele and a band of 6.5 kb for the mutant allele due to the introduced *Eco*RV site in the neo cassette. *Eco*RV/*Xho*I-digested DNAs were hybridized to a 5′ flanking probe (5′probe): An 11.2-kb band was observed for the wild-type allele and a 6.7-kb band for the mutant allele due to the presence

of an *EcoR*V site in the neo cassette. **(c)** Genotyping PCR was used to differentiate to a 203-bp fragment for the wild-type locus, a 250-bp fragment for the floxed allele (with or without neo cassette), and a 320-bp band for the deletion allele. The position of the primers is indicated by the black triangles in **(a). (d)** Comparison of Ndrg4 expression levels in the brain and heart of wild type and mutant mice at 3 weeks of age by Western blot analysis. α-Tublin signal shows similar loading of samples between lanes.

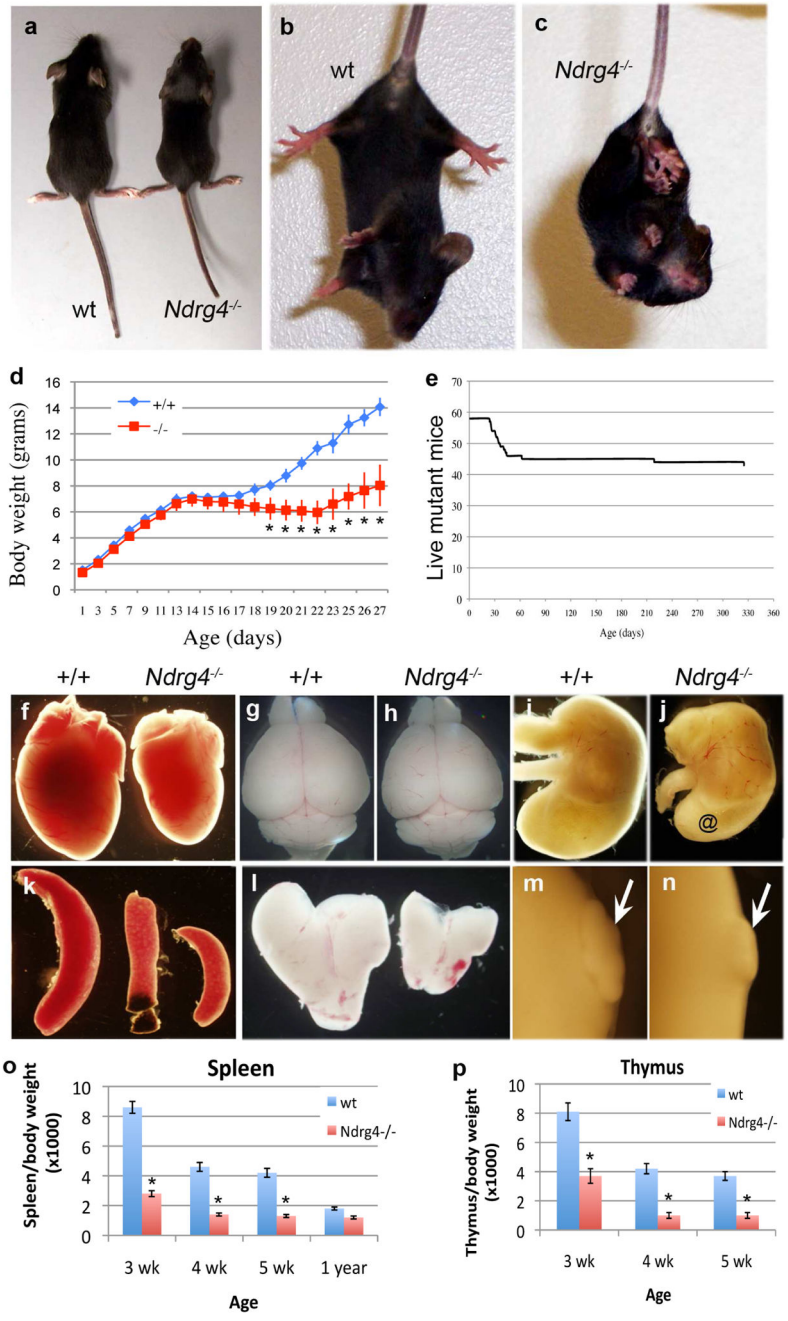

Fig. 2.

Growth retardation and disproportional small spleens and thymuses in *Ndrg4*$^{-/-}$ mice. **(a)** *Ndrg4*$^{-/-}$ mice are relatively smaller than their wt littermates at 3 weeks of age. Compared to a wt littermate **(b)**, an abnormal hind limb clasping phenotype was seen in *Ndrg4*$^{-/-}$ mice at 5 weeks of age upon tail suspension **(c). (d)** Growth curves of wt (n=3), and *Ndrg4*$^{-/-}$ (n=4) mice from a typical litter in 4 weeks. **(e)** Long-term survival of *Ndrg4*$^{-/-}$ mice. 20.7% (12 of 58) of *Ndrg4*$^{-/-}$ mice (n=58) succumbed death between 3 and 6 weeks after birth. Macroscopic appearance of wt and *Ndrg4*$^{-/-}$ hearts **(f)**, wt and *Ndrg4*$^{-/-}$ brain **(g, h)**,

stomach **(i, j)**, spleen **(k)**, thymuses **(l)** and intestinal Peyer's patches (arrows) **(m, n)** at 3 weeks of age. **(o)** Involution of the spleen in wt and *Ndrg4*$^{-/-}$ mice. **(p)** Involution of the thymus in wt and *Ndrg4*$^{-/-}$ mice. Note the shrinkage of forestomach (@) in *Ndrg4*$^{-/-}$ mice. *P < 0.05.

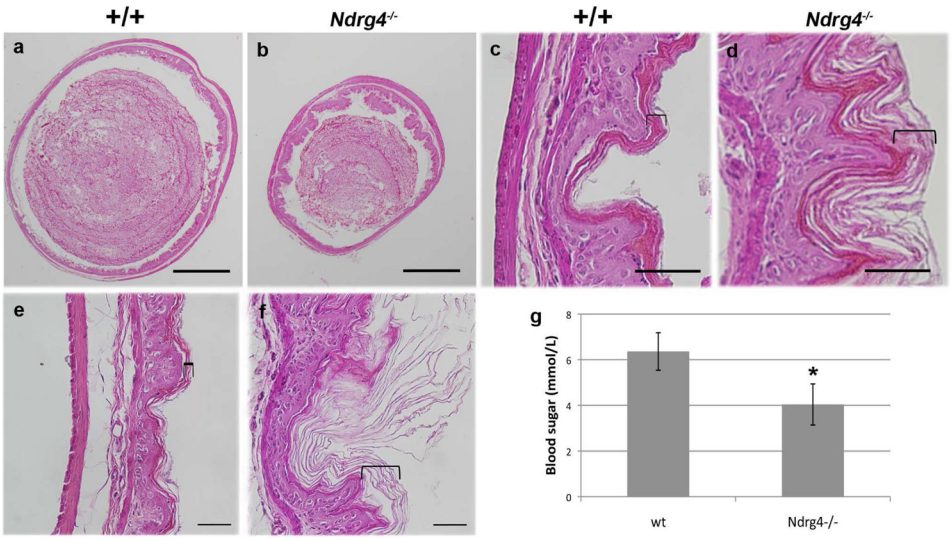

Fig. 3.

Gut phenotype in *Ndrg4*$^{-/-}$ mice. H&E staining of histological sections of forestomach *Ndrg4*$^{-/-}$ mice and their wt littermates at 2 weeks after birth **(a–d)** and at 3 weeks of age **(e, f)** showing excessive hyperkeratosis in *Ndrg4*$^{-/-}$ mice. **(c)** and **(d)** are high-power magnification of **(a)** and **(b)**, respectively. Brackets indicate keratinized layers. Scale bars in **(a, b)**: 500 μm; Scale bars in **(c–f)**: 100 μm. **(g)** Compared to wt littermates (n=5), *Ndrg4*$^{-/-}$ mice (n=5) have reduced blood sugar level at 5 weeks of age. *P < 0.05.

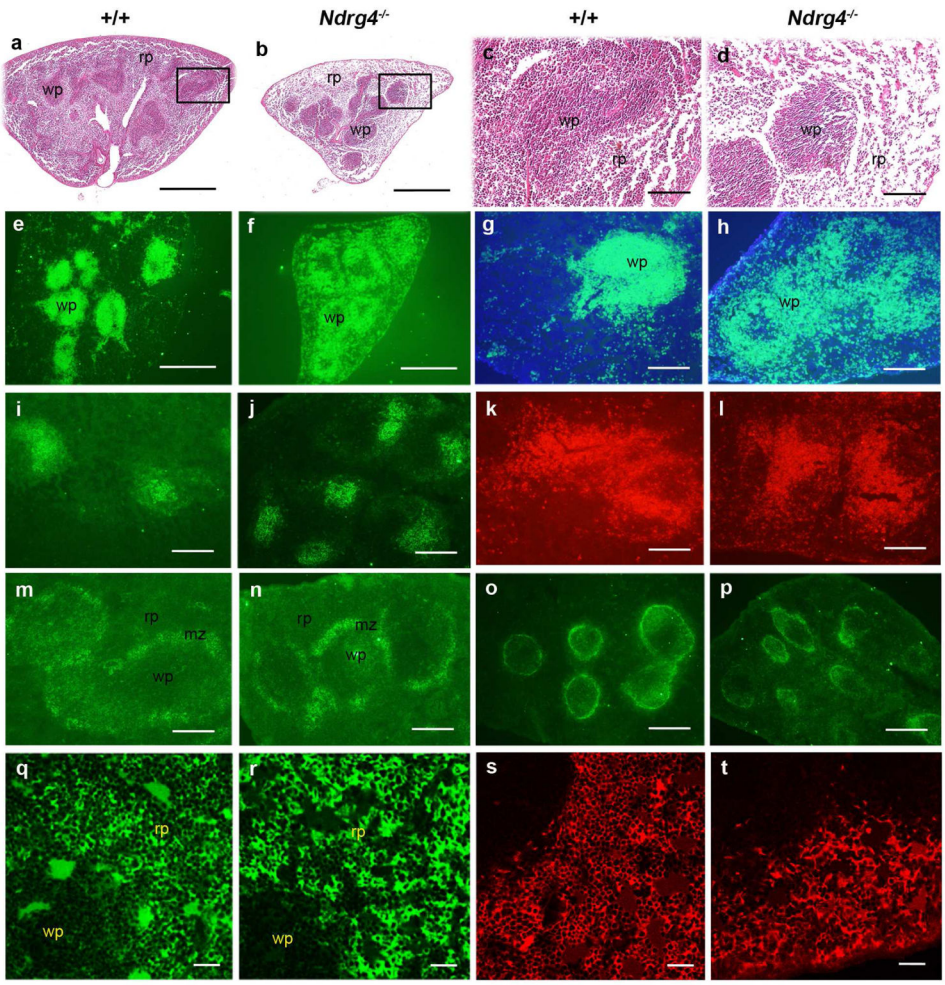

Fig. 4.

Abnormal histology of spleen in the *Ndrg4*$^{-/-}$ mice. Paraffin sections of spleens from wt **(a, c)** and *Ndrg4*$^{-/-}$ mutant **(b, d)** mice were stained with H&E. **(c)** and **(d)** are high-power magnification of the boxed areas in **(a)** and **(b)**, respectively. Although the white pulp (wp) is sharply separated from the red pulp (rp) as in wt, the cell density in the rp of *Ndrg4* mutant mice is reduced. **(e–t)** Cryostat sections from wt **(e, g, i, k, m, o, q, s)** and mutant **(f, h, j, l, n, p, r, t)** spleens at 3 weeks of age were immunostained with specific antibodies: B220 for B cells **(e–h)**, CD35 for follicular dendritic cells **(i, j)**, CD4 for T cells **(k, l)**, SIGN Related 1 (ER-TR-9) for a subpopulation of macrophages in the marginal zone (mz) **(m, n)**, Mucosal vascular addressin-1 (MAdCAM1) for **(o, p)**, F4/80 for macrophages **(q, r)**, and TER119 for erythroid cells **(s, t). (g)** and **(h)** are high-power magnification of **(e)** and **(f)**, respectively. Note the lower density and abnormal morphology of red blood cells in mutant spleen **(t)**. Scale bars in **(a, b)**: 500 μm; Scale bars in **(c–t)**: 100 μm.